Journal of Alloys and Compounds, Volume 653, 25 December 2015, Pages 260–265
DOI:10.1016/j.jallcom.2015.09.034

# Improved electrocaloric effect in (100)-oriented $Pb_{0.97}La_{0.02}(Zr_{0.57}Sn_{0.38}Ti_{0.05})O_3$ antiferroelectric thick film by interface engineering

Ye Zhao[1], Xihong Hao[*,1] , and Qi Zhang[2,3]

1-School of Materials and Metallurgy, Inner Mongolia University of Science and Technology, Baotou 014010, China

2-State Key Laboratory of Advanced Technology for Materials Synthesis and Processing, Wuhan University of Technology, Wuhan 430070, Hubei, China

3-Department of Manufacturing and Materials, Cranfield University, Cranfield, Bedfordshire, MK43 0AL, UK

**Abstract:** In this work, 1.5-μm $Pb_{0.97}La_{0.02}(Zr_{0.57}Sn_{0.38}Ti_{0.05})O_3$ antiferroelectric thick films with and without a $ZrO_2$ thin layer were deposited on $LaNiO_3$(100)/Si(100) substrates. The effects of $ZrO_2$ thin layer on the microstructure, electrical properties, and especial electrocaloric effect of the antiferroelctric films were studied in detail. Although the films both with and without $ZrO_2$ buffer layer displayed (100)-preferred orientation possessed dense and uniform surface microstructure, the $ZrO_2$-buffered films have an enlarged grain size by 27%, compared with the thick films without the buffer layer. Accordingly, the dielectric constant and saturate polarization of this antiferroelectric thick film was improved by the insertion of $ZrO_2$ thin layer, and simultaneously its leakage current was slightly reduced. As a result, a great improvement in cooling character caused by ferroelectric-antiferroelectric phase switching, was realized in the $ZrO_2$-buffered films.

**Keywords:** Antiferroelctric; Thick films; Electrocaloric effect; Interface engineering

*Corresponding author: xhhao@imust.cn; Tel: +86-472-5951572; Fax: +86-472-5951571

## 1. Introduction

The electrocaloric effect (ECE) defined as the change of temperature and entropy in dielectrics upon application or withdrawal of an applied electric field, which attracts a lot of concern from fundamental research [1-3]. It is believed that ECE is a promising and environmental friendly candidate for a broad range of applications including on-chip cooling and temperature regulation for sensors and electronic devices. The first study on ECE was reported in 1930 in Rochelle salt by Kobeko and Kurtschatov [4]. Then lots of interests were focused on the ECE in bulk ceramics and liquids in the 1960s and 1970s, but no commercial value was exploited due to the small ECE and low operating temperature [5-6]. Until 2006, the turn was come after the reporting giant ECE of 12 K at 25 V in 350-nm-thick $PbZr_{0.95}Ti_{0.05}O_3$ film [7]. Intrigued by this result, numerous works on ECE were carried out in ferroelectric (FE) ceramics and polymers in the forms of bulk, film and, recently, composite [8-11]. Generally, the largest ECE is always realized near the phase transition temperature, such as FE-paraelectric (PE) switching point, also called the Curie temperature ($T_c$). However, $T_c$ in some FEs is well above room temperature, which is not favor for their practical applications.

Compared with FEs, antiferroelectric (AFE) materials possess more abundant phase transition behavior. It is well known that the phase transition between AFE and FE could be easily happened under the function of external fields such as electric field, stress and temperature, which can be carried out near the room temperature [12,13]. A larger change of entropy is also produced during this kind of phase transition. Therefore, it is reasonably predicated that outstanding ECEs can also be realized at room temperature during the phase transition between AFE and FE. The first work on the ECE in AFEs was reported by Thacher in 1968, in which a temperature change of $\Delta T$ = 1.6 K at 328 K in $Pb(Zr_{0.455}Sn_{0.455}Ti_{0.09})O_3$ bulk ceramic was observed during FE-AFE phase switching [14]. The corresponding ECE coefficient $\xi$ defined as $\Delta T/\Delta E$ was 0.047 K·cm/kV, which was comparable with the optimum values in recently exploited FE materials. Thus, it could be concluded that AFEs

in film form should display excellent ECE, because of its good electric-field endurance. As expected, a giant ECE peak ($\Delta T$ =45.3 K and $\Delta T/\Delta E$=0.076 K·cm/kV) at room temperature was reported in a 320-nm-thick $Pb_{0.8}Ba_{0.2}ZrO_3$ (PBZ) thin film [15]. More recently, considerable ECEs ($\Delta T$ =35.0 K and $\Delta T/\Delta E$=0.039 K·cm/kV) at room temperature were also achieved during FE-AFE phase switching in our 2-μm-$Pb_{0.97}La_{0.02}(Zr_{0.75}Sn_{0.18}Ti_{0.07})O_3$ AFE thick film [16]. Due to its giant ECE near room temperature, it could be concluded that AFEs are more likely to be used in practice, in contrast to its FE counterpart. However, currently, the studies on ECE in AFEs are rarely reported and thus it is necessary to do a further investigation systemically.

It is well known that the diffusion between dielectric films and electrodes is a main contribution to the degradation of the electrical properties and that the interface engineering is widely employed to overcome this kind of shortcoming. It was reported that, by inserting a thin oxide film (such as $TiO_2$, $Al_2O_3$, $CeO_2$, $SiO_2$ and $ZrO_2$, etc.) between FE films and the bottom electrodes, the dielectric and polar properties of the films could be greatly enhanced [17-20]. Moreover, ECE has a close relation with the polar performance of AFEs and FEs. Generally, larger polarization values lead to an improved ECE [21]. To the best of our knowledge, there is no report on the improvement of ECE through the interface engineering. Thus, in this work, in order to optimize ECE of AFE films, a very thin $ZrO_2$ film was firstly prepared on the bottom electrodes before the disposition of AFE thick films with a chemical composition of $Pb_{0.97}La_{0.02}(Zr_{0.57}Sn_{0.38}Ti_{0.05})O_3$, which was located in tetragonal region in the corresponding ternary phase diagram. The advantages of thick films lie both in higher critical breakdown field like thin films and in larger volume like bulk ceramics.

**2. Experimental procedure**

The fabrication of $Pb_{0.97}La_{0.02}(Zr_{0.57}Sn_{0.38}Ti_{0.05})O_3$ (shorted as PLZST 2/57/38/5) thick films was from a sol-gel route, which was similar to our recent work [22]. Lead acetate trihydrate [$Pb(CH_3COO)_2 \cdot 3H_2O$], lanthanum acetate [$La(CH_3COO)_3$], tin acetate [$Sn(CH_3COO)_4$], titanium

isopropoxide [$Ti(OCH(CH_3)_2)_4$] and zirconium isopropoxide [$Zr(OC_3H_7)_4$)] were used as the starting raw materials. Glacial acetic and deionized water were used as solvents. At first, lead acetate trihydrate, tin acetate, lanthanum acetate hydrate, and acetic acid were mixed in a ratio according to the predetermined number. The mixed solution was distilled at 110 $^oC$ for 30 min to remove water. When the mixed solution was cooled to room temperature, zirconium propoxide and titanium isopropoxide were added and stirred for 30 min. During the mixing process deionized water was added in the proportion of one mole of deionized water to five moles of lead to stabilize the solution. Then lactic acid functioned as catalyzer and chelation agent was added into the solution in the ratio of one mole of lactic acid to one mole of lead. Meanwhile, in order to improve the mechanical properties of the gel film, ethylene glycol was also added into the solution in the ratio of one mole of ethylene glycol to one mole of lead. The solution was synthesized after mixing for 1 h at room temperature, and the final concentration of the solution was 0.5 M. 20 mol% excess of lead acetate trihydrate was introduced to compensate the lead loss during annealing and to prevent the formation of pyrochlore phase in the film.

The conductive $LaNiO_3$ (LNO) films with a thickness of about 400 nm were chosen as bottom electrodes, which were prepared on Si (100) substrates by the chemical solution deposition route and as described in Ref. 23. The Si (100) substrate was first cleaned and annealed at 700 $^oC$ for 10 min before the LNO film was deposited on the substrate. The obtained LNO films showed a (100) growth orientation. After aging of the sol for 24 h, PLZST 2/57/38/5 AFE thick film was deposited on $ZrO_2$ buffer layered LNO/Si (100) substrate by a multiple-layer spin-coating procedure. For comparison, PLZST 2/57/38/5 AFE thick film was also directly grown on LNO/Si (100) substrate without buffer layer. Each wet PLZST layer was spin-coated at 3000 rpm for 40 s. In order to reduce the formation of cracks, each wet film was first dried at 350 $^oC$ for 10 min and subsequently pyrolyzed at 600 $^oC$ for 10 min. The spin-coating and heat-treatment were repeated several times to obtain the desired thickness. To prevent excessive lead loss and form pure perovskite phase, a

capping layer of 0.4 M PbO precursor solution which was prepared from lead acetate trihydrate was deposited on the top of the PLZST 2/57/38/5 films before it went through a final anneal at 700 $^{o}$C for 30 min. The final thickness of the PLZST AFE thick films was about 1.5 μm, determined from the cross-sectional images.

Here, it should be noted that $ZrO_2$ buffer layer on LNO/Si (100) substrate was also prepared through a sol-gel route. Zirconium propoxide was employed as the starting raw material. 2-methoxyethanol and acetylacetone were used as the solvent and stabilizer, respectively. The mole ratio between acetylacetone and Zr was 2. The solution was synthesized after mixing for 1 h at room temperature, and the final concentration of the solution was 0.02 M. After aging of the ZrO2 sol for 24 h, $ZrO_2$ buffer layer was deposited on LNO/Si (100) substrate by the similar spin-coating procedure. In order to control the thickness of the buffer layer, only one layer was spin-coated at 3000 rpm for 20 s. Finally, the buffer layer was obtained after beinganneal at 700 $^{o}$C for 10 min. As reported earlier, the thickness of $ZrO_2$ buffer layer was about 5 nm [24].

The microstructures of these AFE thick films were analyzed by X-ray diffraction (XRD Bruker D8 Advanced Diffractometer, German) and field-emission scanning electron microscopy (FE-SEM ZEISS Supra 55, German), respectively. For the electrical measurements, gold pads of 0.20 mm in diameter were coated on the film surface as top electrodes by using a DC sputtering method. The frequency and temperature-dependent dielectric properties of the films were measured by using a computer-controlled Agilent E4980A *LCR* analyzer. The bipolar polarization-electric field hysteresis (*P-E*) loops at 1 kHz and the leakage current characteristic of the films were measured by a Ferroelectric tester (Radiant Technologies, Inc., Albuquerque, NM). ECE of the films was calculated according to the *P-E* results.

**3. Results and discussion**

Fig. 1 shows the XRD patterns of PLZST 2/57/38/5 AFE thick films on LNO/Si(100) substrates with and without $ZrO_2$ buffer layer after beinganneal at 700 $^{o}$C. For convenience, the

lattice indexes of the diffraction peaks are labeled as pseudocubic structure rather than tetragonal phase. Both the thick films had crystallized into a pure perovskite phase, and no secondary phase was detected. Apparently, the AFE thick films deposited on LNO(100)/Si(100) substrates also show well (100)-preferred orientation, which is due to the same pseudocubic perovskite structure and the small lattice mismatch between AFE thick films and LNO bottom electrodes. The similar work was also reported in other lead-based FE and AFE films deposited on LNO bottom electrodes [25,26]. The insert in Fig. 1 shows the surface images of the PLZST 2/57/38/5 AFE thick films with and without $ZrO_2$ buffer layer. Evidently, both the films display dense and uniform microstructures and no micro-cracks or other micro-structural defects are found in the films, which is ascribed to the two-step heat-treatment procedure for the thick film preparation. The average grain size is about 461 and 586 nm for AFE thick films without and with $ZrO_2$ buffer layer, respectively, which was calculated by using the Nano Measurer software. It means that the insert of $ZrO_2$ layer leads to an enlarged grain size by 27%, compared with the thick films without the buffer layer. The reason for the larger grain size of AFE thick film can be explained by the decrease in nucleation energy during the film growth process caused by $ZrO_2$ buffer layer. The similar results were also observed in other FE and AFE films with oxide buffer layer [27, 28]. It could be predicted that the enlarged grains have a strong effect on the final electrical properties of AFE films.

Temperature dependences of the relative dielectric constant for PLZST 2/57/38/5 AFE thick films with and without $ZrO_2$ buffer layer are presented in Fig. 2, which were measured at 100 kHz on heating process. Obviously, both the AFE thick films show only one dielectric peak during the heating process and no other phase transformation are checked. The relative dielectric constant in the both cases first increases gradually, and then decreases with the temperature increasing. The dielectric peaks corresponding to the transition from AFE to PE phase, which are the so-called $T_c$, are observed at 158 and 164 $^oC$ for the thick films without and with $ZrO_2$ buffer layer, respectively. The slightly raised $T_c$ value may be ascribed to the larger grain size for AFE films with $ZrO_2$ buffer

layer. It was reported that declined grain size usually led to a decrease of $T_c$ [29]. The insert in Fig. 2 presents the frequency-dependent relative dielectric constant and dielectric loss of the both AFE thick films, which were measured at room temperature and over 1-1000 kHz. With the increase of frequency, the relative dielectric constant for the both samples is slightly decreased, which is contributed to the polarization relaxor for the various dipoles [30]. Moreover, it can be found that the AFE thick films with $ZrO_2$ buffer layer have a larger dielectric constant, compared with the films without buffer layer. For example, the relative dielectric constants at 1, 10, 100, 1000 kHz are 515, 404, 491, 455 and 654, 653, 642, 622 for AFE thick films without and with $ZrO_2$ buffer layer, respectively. The similar results were also reported in $TiO_2$-buffered (Ba,Sr)$TiO_3$ FE thin films and $CeO_2$-buffered (Pb,La)(Zr,Sn,Ti)$O_3$ AFE thin films [31,32]. It is supposed to be caused by the enlarged grain size for the oxide-buffered films. Different from their relative dielectric constant, both the thick films show the similar dielectric loss. The loss tangent is less than 0.02 at the frequency below 100 kHz, and greatly enhances at the frequency above 100 kHz. The large loss tangent values at high measurement frequency are often observed in AFE and FE films with oxide electrodes such as LNO, which is caused by the larger resistance of this kind of electrodes [33].

The room temperature *P-E* loops of the thick films are shown in Fig. 3, which were measured at 1 kHz. Both samples display a well-developed double hysteresis loop, demonstrating their AFE nature. A small remnant polarization of 3.5 μC/cm$^2$ was detected in the two samples, which should be caused by the interface layer, space charge, unstable AFE regions, and so on. Under the measurement condition, the corresponding maximum polarization for the films with and without $ZrO_2$ buffer layer is 60 and 49 μC/cm$^2$, respectively. The improved polarization value for AFE thick film with $ZrO_2$ buffer layer is resulted from its larger relative dielectric constant because the polarization ($P$) is equal to $\varepsilon_0(\varepsilon_r\text{-}1)E$ (where $\varepsilon_0$ is permittivity of free space, $\varepsilon_r$ is the relative dielectric constant and $E$ is the applied electric field). The insert in Fig. 3 shows the corresponding electric field $E$-dependent $\frac{\partial P}{\partial E}$ values. The magnitude of the phase switching fields can be

determined from the peaks in $\frac{\partial P}{\partial E}$-$E$ curves. Accordingly, the AFE-FE switching field is approximately 243 and 226 kV/cm for PLZST 2/57/38/5 AFE thick films without and with $ZrO_2$ buffer layer, respectively, and the corresponding FE-AFE field is 163 and 142 kV/cm. This means that the insert of $ZrO_2$ layer makes the phase swathing much easier.

Fig. 4(a) shows the adiabatic temperature change $\Delta T$ of the both AFE thick films under the electric field $E$=900 kV/cm. Assuming the Maxwell relation $\left(\frac{\partial P}{\partial T}\right)_E = \left(\frac{\partial S}{\partial E}\right)_T$, the reversible changes of $\Delta T$ a material of density ($\rho$) with specific heat capacity($C$) are expressed by [34]:

$$\Delta T = -\frac{1}{C\rho}\int_{E_1}^{E_2} T\left(\frac{\partial P}{\partial T}\right)_E dE \quad , \qquad (1),$$

where $T$ is absolute temperature, $P$ is maximum polarization at applied electric field $E$, $E_1$ and $E_2$ are the initial and final applied electric field. Here $E_1$ = 0 and $E_2 = E$; thus $\Delta E$ is equal to $E$. The specific heat capacity $C$ = 330 $J \cdot K^{-1} \cdot kg^{-1}$ and the theoretical density $\rho$ = 8.3 $g \cdot cm^{-3}$ are selected for these thick films as reported before [35]. As expected, the large $\Delta T$ in both films are received in a wide range of near the room temperature, which is induced by the phase transition of FE-AFE. The values of $\Delta T$ at 21 $^oC$ are 27.3 and 37.1 $^oC$ for PLZST 2/57/38/5 AFE thick films without and with $ZrO_2$ buffer layer, respectively. With the operating temperature increasing, the $\Delta T$ firstly decreases, indicating a reduction of entropy change between AFE and FE phase transition. With the further increase of temperature, a peak of $\Delta T$ = 7.8 and 7.2 $^oC$ is detected at 143 and 150 $^oC$ for the AFE thick films without and with $ZrO_2$ buffer layer, respectively, which is believed to be caused by the AFE-PE phase transition. The temperature corresponding to the peak of $\Delta T$ is slightly below its $T_c$, which is consistent with that previously reported by Tatsuzaki, because the spontaneous value of $P$ greatly changes with temperature below $T_c$ [36]. In fact, ECE can occur both above and below $T_c$, but the microscopic models of ECEs are not well established [7]. For the cooling application, apart from large $\Delta T$, higher entropy change $\Delta S$ is also desired, which can be expressed as [37]:

$$\Delta S = -\frac{1}{\rho}\int_{E_1}^{E_2}\left(\frac{\partial P}{\partial T}\right)_E \mathrm{d}E \quad (2).$$

Fig. 4(b) shows the corresponding adiabatic entropy changes $\Delta S$ of the AFE thick films. Clearly, large entropy change could occur during the FE-AFE and AFE-PE phase transition. The maximum $\Delta S$ value is obtained at 21 $^{o}$C, which is 31 and 42 $J \cdot K^{-1} \cdot kg^{-1}$ for the AFE thick films without and with $ZrO_2$ buffer layer, respectively. Based on the results, it can be clearly found that ECE of the AFE thick films is greatly improved by the insert of $ZrO_2$ layer.

Fig. 5(a) and 5(b) display the leakage current density-time characteristics of the PLZST 2/57/38/5 AFE thick films without and with $ZrO_2$ buffer layer, which were measured at 600 kV/cm and at different temperature (25, 75, 150, and 200 $^{o}$C). The leakage current density shows strong initial time-dependence because of the dielectric polarization relaxation, which obeys the Curie-von Schweidler law as follows [38]:

$$J = J_s + J_0 \times t^{-n} \quad (3),$$

where $J_s$ is the steady-state current density, $J_0$ a fitting constant, $t$ the relaxation time in second, and $n$ the slope of the log-log plot. The possible mechanisms are associated with the Curie-von Schweidler law: space charge trapping, relaxation time distribution and electrical charge hopping [38]. Evidently, with the temperature increasing, the steady-state leakage current density increases for both samples, which is caused by the enhanced mobility of charge carriers at the elevated temperature. However, in the measurement temperature range, the leakage current density of PLZST 2/57/38/5 AFE thick films with $ZrO_2$ buffer layer is always lower than that of the films without buffer layer. For example, by fitting the leakage current density data into Eq. 3, the steady-state leakage current density $J_s$ at 25 $^{o}$C is $8.2\times10^{-7}$ and $1.4\times10^{-7}$ A/cm$^2$ for the AFE films without and with $ZrO_2$ buffer layer, respectively. This result indicates that the addition of $ZrO_2$ layer is also helpful to reduce the leakage current of the films, which is favor to the decrease of energy loss in practical application. It was reported that the steady-state leakage current density of

lead-based FE and AFE films can be fitted into the Arrhenius relationship, which could be expressed as [39]:

$$J_s = C\exp\left(-\frac{E_a}{kT}\right) \quad (4),$$

where $C$ is a fitting constant, $E_a$ the activation energy, $k$ the Boltzmann constant. According to the fitting curve showed in the inset of Fig. 5(a) and 5(b), the obtained activation energy $E_a$ is 0.37 and 0.41 eV for AFE thick films without and with $ZrO_2$ buffer layer, respectively. These values are similar to the reported results in lead-based AFE and FE films [40,41]. It is supposed that the first ionization of oxygen vacancies is responsible for the conduction of the films, when the activation energy is within the range 0.32-0.49 eV [42]. The slightly increased activation energy for the $ZrO_2$-buffered AFE films should be attributed to the $ZrO_2$ layer blocking the mobile ionic defects and reducing the free charge carriers to transport.

**4. Conclusion**

Both (100)-oriented and uniformed PLZST 2/57/38/5 AFE thick films with and without $ZrO_2$ buffer layer were successfully prepared on LNO bottom electrodes. It was observed that the grain size of the thick film increased from 461 nm to 586 nm by the insert of $ZrO_2$ layer. As compared with AFE thick films without $ZrO_2$ buffer layer, the $ZrO_2$-buffered films have an enhanced relative dielectric constant and polarization value, but a declined leakage current density. Accordingly, an improved ECE was obtained in the $ZrO_2$-buffered AFE thick films. The reversible temperature changes $\Delta T$ at 21 $^{o}$C are 27.3 and 37.1 $^{o}$C for PLZST 2/57/38/5 AFE thick films without and with $ZrO_2$ buffer layer, respectively, and the corresponding entropy changes $\Delta S$ are 31 and 42 $J \cdot K^{-1} \cdot kg^{-1}$. The result indicates that interface engineer is an efficient way to optimize the cooling property of AFE films.

**Acknowledgements**

The authors would like to acknowledge the financial support from the Ministry of Sciences and

Technology of China through 973-project under grant No.2014CB660811, the National Natural Science Foundation of China under grant No. 51462027, and the Innovation Fund of Inner Monglia University of Science and Technology No. 2014QNGG01.

**Reference**


[1] X. Moya, E. Stern-Taulats, S. Crossley, D. González-Alonso, S. Kar-Narayan, A. Planes, L. Mañosa, N.D. Mathur, Giant electrocaloric strength in single-crystal $BaTiO_3$, Adv. Mater. **25** (2013) 1360-1365.

[2] S. Lang, Cryogenic refrigeration utilizing the electrocaloric effect in pyroelectric lithium sulfate monohydrate, Ferroelectrics **11** (1976) 519-523.

[3] X.S. Qian, H.J. Ye, Y.T. Zhang, H.M. Gu, X.Y. Li, C.A. Randall, Q.M. Zhang, Giant electrocaloric response over a broad temperature range in modified $BaTiO_3$ ceramics, Adv. Funct. Mater. **24** (2014) 1300-1305.

[4] P. Kobeko, J. Kurtschatov, Dielektrische eigenschaften der seignettesalzkristalle, Z. Phys. **66** (1930) 192-205.

[5] B.A. Tuttle, D.A. Payne, The effects of microstructure on the electrocaloric properties of $Pb(Zr,Sn,Ti)O_3$ ceramics, Ferroelectrics **37** (1981) 603-606.

[6] W.N. Lawless, A.J. Morrow, Specific heat and electrocaloric properties of a $SrTiO_3$ ceramic at low temperatures, Ferroelectrics **15** (1977) 159-165.

[7] A.S. Mischenko, Q. Zhang, J.F. Scott, R.W. Whatmore, N.D. Mathur, Giant electrocaloric effect in thin films $PbZr_{0.95}Ti_{0.05}O_3$, Science **311** (2006) 1270-1271.

[8] A.S. Mischenko, Q. Zhang, R.W. Whatmore, N.D. Mathur, Giant electrocaloric effect in the thin film relaxor ferroelectric $0.9PbMg_{1/3}Nb_{2/3}O_3$-$0.1PbTiO_3$ near room temperature, Appl. Phys. Lett. **89** (2006) 242912.

[9] D.Q. Xiao, Y.C. Wang, R.L. Zhang, S.Q. Peng, J.G. Zhu, B. Yang, Electrocaloric properties of $(1-x)Pb(Mg_{1/3}Nb_{2/3})O_3$-$xPbTiO_3$ ferroelectric ceramics near room temperature, Mater. Chem. Phys. **57** (1998) 182-185.

[10] B. Neese, S.G. Lu, B.J. Chu, Q.M. Zhang, Electrocaloric effect of the relaxor ferroelectric poly(vinylidene fluoride-trifluoroethylene-chlorofluoroethylene) terpolymer, Appl. Phys. Lett.

**94** (2009) 042910.

[11] S.G. Lu, Q.M. Zhang, Electrocaloric Materials for solid-state refrigeration, Adv. Mater. **21** (2009) 1983-1987.

[12] X.H. Hao, J.W. Zhai, Electric-field tunable electrocaloric effects from phase transition between antiferroelectric and ferroelectric phase, Appl. Phys. Lett. **104** (2013) 022902.

[13] X.H. Hao, J.W. Zhai, L.B. Kong, Z.K. Xu, A comprehensive review on the progress of lead zirconate-based antiferroelectric materials, Prog. Mater. Sci. **63** (2014) 1-57.

[14] P.D. Thacher, Electrocaloric effects in some ferroelectric and antiferroelectric $Pb(Zr,Ti)O_3$ compounds, J. Appl. Phys. **39** (1968) 1996-2002.

[15] B.L. Peng, H.Q. Fan, Q. Zhang, A giant eletrocaloric effect in nanoscale antiferroelectric phase coexisting in a relaxor $Pb_{0.8}Ba_{0.2}ZrO_3$ thin films at room temperature, Adv. Funct. Mater. **23** (2013) 2987-2992.

[16] Y. Zhao, X.H. Hao, Q. Zhang, A giant electrocaloric effect of a $Pb_{0.97}La_{0.02}(Zr_{0.75}Sn_{0.18}Ti_{0.07})O_3$ antiferroelectric thick film at room temperature, J. Mater. Chem. C **3** (2015) 1694-1699.

[17] W. D. Yang, and S. M. Haile, Characterization and microstructure of highly preferred oriented lead barium titanate thin films on MgO (100) by sol-gel process, Thin Solid Films **510** (2006) 55-61.

[18] H.S. Choi，G.S. Lim, J.H. Lee, Y.T. Kim, S.I. Kim, D.C. Yoo, J.Y. Lee, I.H. Choi, Improvement of electrical properties of ferroelectric gate oxides structure by using $Al_2O_3$ thin films as bueffer insulator, Thin Solid Films **444** (2003) 276-281.

[19] Y. Lin, B.R. Zhao, H.B. Peng, B. Xu, H. Chen, F. Wu, H.J. Tao, Z.X. Zhao, J.S. Chen, Growth and polarization features of highly (100) oriented Pb $(Zr_{0.53}Ti_{0.47})O_3$ films on Si with ultrathin $SiO_2$ buffer layer, Appl. Phys. Lett. **73** (1998) 2781.

[20] W.C. Shih, Z.Z. Yen, Y.S. Liang, Preparation of highly *C*-axis-oriented PZT films on Si substrate with MgO buffer layer by the sol-gel method, J. Phys. Chem. Solids **69** (2008)

593-596.

[21] R. Pirc, Z. Kutnjak, R. Blinc, Upper bounds on the electrocaloric effect in polar solids, Appl. Phys. Lett. **98** (2011) 021909.

[22] X.H. Hao, Y. Wang, L. Zhang, L.W. Zhang, S.L. An, Composition-dependent dielectric and energy-storage-properties of (Pb,La)(Zr,Sn,Ti)$O_3$ antiferroelectric thick films, Appl. Phys. Lett. **102** (2013) 163903.

[23] X.J. Meng, J.L. Sun, J. Yu, H.J. Ye, S.L. Guo, J. H. Chu, Preparation of highly (100)-oriented metallic $LaNiO_3$ films on Si substrates by a modifed metalorganic decomposition technique. Appl. Surf. Sci. **171** (2001) 68-70.

[24] X.H. Hao, J.W. Zhai, J.B. Xu, X. Yao, Preparation of PLZT antiferroelectric thin films on $ZrO_2$ buffered substrates, Ferroelectrics, **357** (2007) 253-258.

[25] N. Sama, C. Soyer, D. Remiens, C. Verrue, R. Bouregba, Bottom and top electrodes nature and PZT film thickness influence on electrical properties, Sensors and Actuators A **158** (2010) 99-105.

[26] Y. Zhao, X.H. Hao, Q. Zhang, Energy-storage properties and electrocaloric effect of $Pb_{(1-3x/2)}La_xZr_{0.85}Ti_{0.15}O_3$ antiferroelectric thick films, ACS Appl. Mater. Interfaces **6** (2014) 11633-11639.

[27] L.L. Chen, M.R. Shen, L. Fang, Y. Xu, Microstructure control of (Pb,Sr)$TiO_3$ films on Pt/Ti/$SiO_2$/Si substrates by a $TiO_2$ buffer layer, Thin Solid Films **516** (2008) 1285-1289.

[28] X.H. Hao, J.W. Zhai, X. Yao, Improved dielectric properties of (110)-preferred (Pb,La)(Zr,Sn,Ti))$O_3$ antiferroelectric thin films on metalorganic decomposition-derived $LaNiO_3$ buffer layer, J. Cryst. Growth **311** (2008) 90-94.

[29] Uchino K. Ferroelectric Devices. New York: Marcel Dekker, 2000.

[30] X.H. Hao, Y. Wang, J.C. Yang, S.L. An, J.B. Xu, High energy-storage performance in $Pb_{0.91}La_{0.09}(Zr_{0.65}Ti_{0.38})O_3$ relaxor ferroelectric thin films, J. Appl. Phys. **112** (2012) 114111.

[31] L.H. Yan, G.S. Wang, X.L. Dong, D. Rémiens, Effects of ultrathin $TiO_x$ seeding layer on crystalline orientation and electrical properties of sputtered (Ba,Sr)$TiO_3$ thin films, J. Am. Ceram . Soc. **93** (2010) 2136-2139.

[32] X.H. Hao, J.W. Zhai, Z.X. Yue, J. Zhou, J.C. Yang, S.L. An, Effects of oxide buffer layers on the microstructure and electrical properties of PLZST 2/87/10/3 antiferroelectric thin films, J. Cryst. Growth **314** (2011) 151-156.

[33] X.H. Hao, J.W. Zhai, Q.P. Jia, B. Shen, X. Yao, Temperature and frequency dependence of dielectric properties of (Pb,La)(Zr,Sn,Ti)$O_3$ antiferroelectric thin films on $LaNiO_3$ bottom electrode with different sheet resistance, J. Phys. D: Appl. Phys. **41** (2008) 165403.

[34] T.M. Correia, J.S. Young, R.W. Whatmore, J.F. Scott, N.D. Mathur, Q. Zhang, Investigation of the electrocaloric effect in a $PbMg_{1/2}Nb_{2/3}O_3$-$PbTiO_3$ relaxor thin film, Appl. Phys. Lett. **95** (2009) 182904.

[35] X.H. Hao, Z.X. Yue, J.B. Xu, S.L. An, C.W. Nan, Energy-storage performance and electrocaloric effect in (100)-oriented $Pb_{0.97}La_{0.02}(Zr_{0.95}Ti_{0.05})O_3$ antiferroelectric thick films, J. Appl. Phys. **110** (2011) 064109.

[36] T. Mitsui, I. Tatsuzaki, and E. Nakamura, "An introduction to the physics of ferroelectrics", Gordon and Breach, Landon, 1976.

[37] B. Neese, B.J. Chu, S.G. Lu, Y. Wang, E. Furman, Q.M. Zhang, Large electrocaloric effect in ferroelectric polymers near room temperature, Science **321** (2008) 821-823.

[38] B.H. Ma, D.K. Kwon, M. Narayanan, U.B. Balachandran, Leakage current characteristics and dielectric breakdown of antiferroelectric $Pb_{0.92}La_{0.08}Zr_{0.95}Ti_{0.05}O_3$ film capacitors grown on metal foils, J. Phys. D: Appl. Phys. **41** (2008) 205003.

[39] S.S. Liu, B.H. Ma, M. Narayanan, S.Tong, R.E. Koritala, U. alachandran, D.L. Shi, Dielectric proper ties of lead lanthanum zirconate titanate thin films with and without $ZrO_2$ inser tion layers, J. Appl. Phys. **113** (2013) 174107.

[40] S. Tong, B.H. Ma, M. Narayanan, S.S. Liu, R.E. Koritala, Z.Q. Hu, Uthamalingam Balachandran, Lead lanthanum zirconate titanate ceramic thin films for energy storage, ACS Appl. Mater. Interfaces **5** (2013) 1474-1480.

[41] X.H. Hao, Y. Zhao, S.L. An, Giant thermal-electrical energy harvesting effect of $Pb_{0.97}La_{0.02}(Zr_{0.75}Sn_{0.18}Ti_{0.07})O_3$ aniferroelectric thick film, J. Am. Ceram . Soc. **98** (2015) 361-365.

[42] Z.Q. Hu, B.H. Ma, R.E. Koritala, U. Balachandran, Temperature-dependent energy storage properties of antiferroelectric $Pb_{0.96}La_{0.04}Zr_{0.98}Ti_{0.02}O_3$ thin films, Appl. Phys. Lett. **104** (2014) 263902.

**Figure Caption**

Fig. 1 XRD patterns of PLZST 2/57/38/5 AFE thick films without and with $ZrO_2$ buffer layer, respectively. The insert is the corresponding surface SEM images.

Fig.2 The temperature-dependent relative dielectric constant of PLZST 2/57/38/5 AFE thick films without and with $ZrO_2$ buffer layer, respectively. The insert is the frequency-dependent relative dielectric constant and dielectric loss of both thick films.

Fig. 3 Room temperature *P-E* loops of PLZST 2/57/38/5 AFE thick films without and with $ZrO_2$ buffer layer, respectively. The insert is the corresponding $\frac{\partial P}{\partial E}$-*E* curves.

Fig. 4 (a) Temperature change of $\Delta T$ as a function of temperature at 900 kV/cm of the PLZST 2/57/38/5 AFE thick films without and with $ZrO_2$ buffer layer, respectively, and (b) the corresponding adiabatic changes in entropy $\Delta S$ of the films.

Fig.5 The temperature-dependent leakage current density and corresponding fitting curve of the PLZST 2/57/38/5 AFE thick films without (a) and with $ZrO_2$ buffer layer (b). The insert is the corresponding steady-state leakage current density and corresponding fitting curve as a function of reciprocal temperature.

Fig. 1 Xihong Hao, and Ye Zhao, *et. al.*

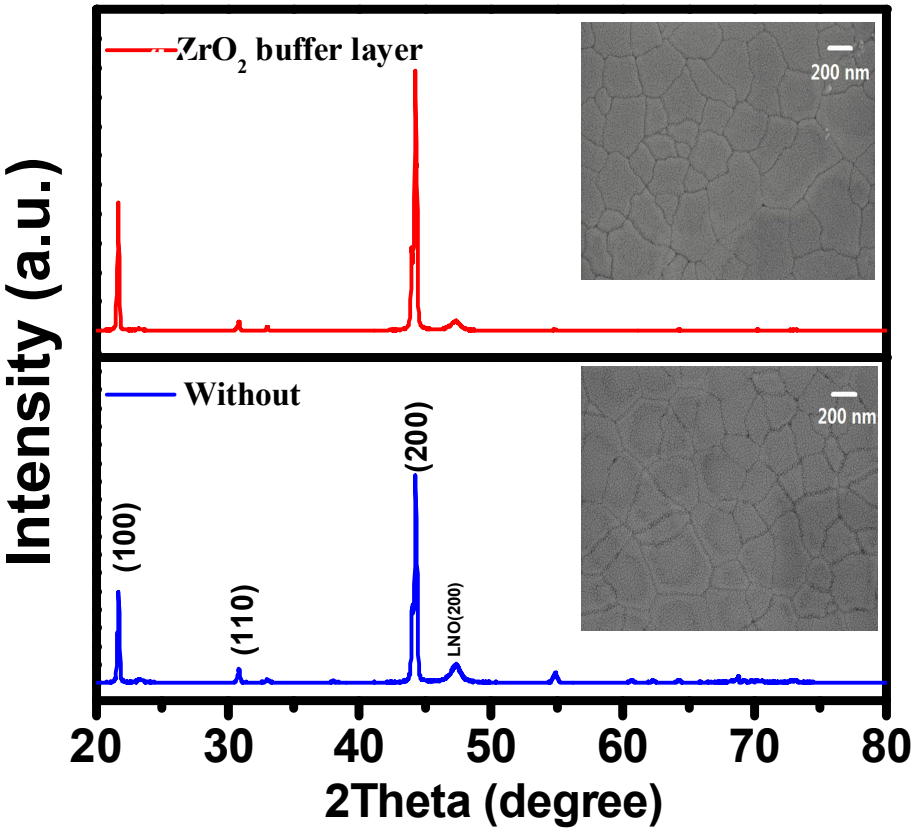

Fig. 2 Xihong Hao, and Ye Zhao, *et. al.*

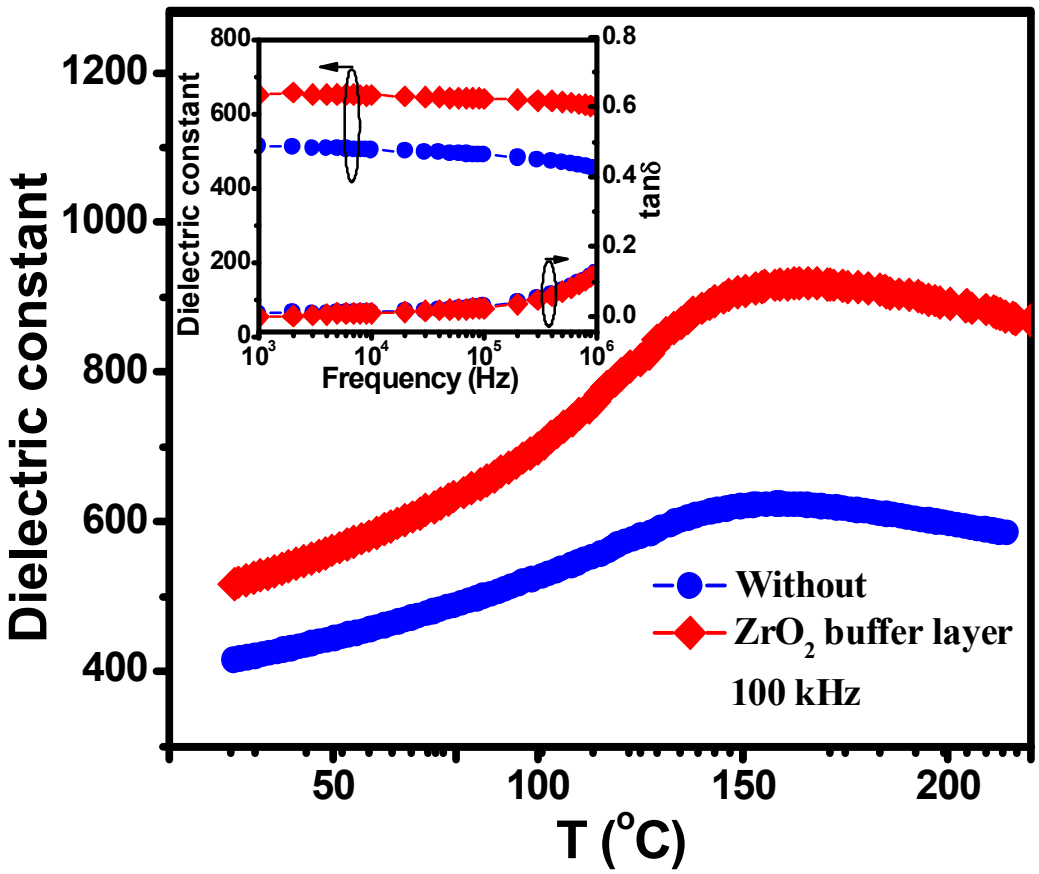

Fig. 3 Xihong Hao, and Ye Zhao, *et. al.*

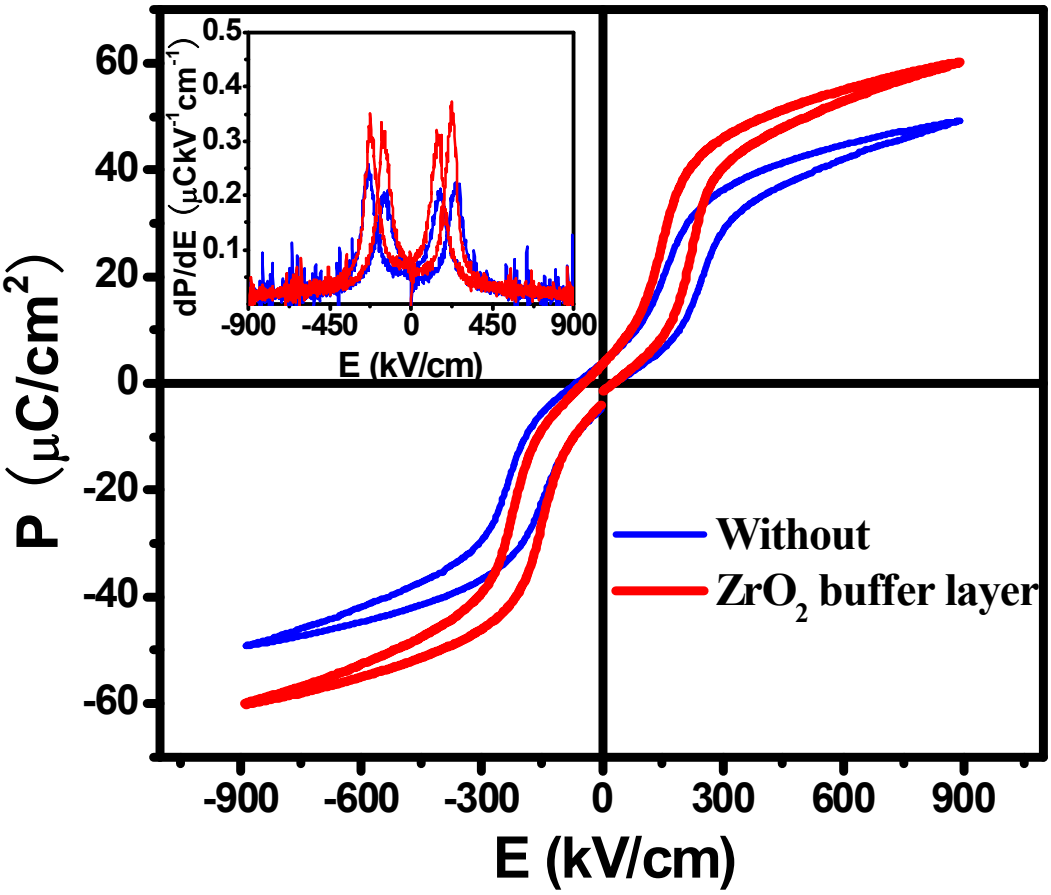

Fig. 4 Xihong Hao, and Ye Zhao, *et. al.*

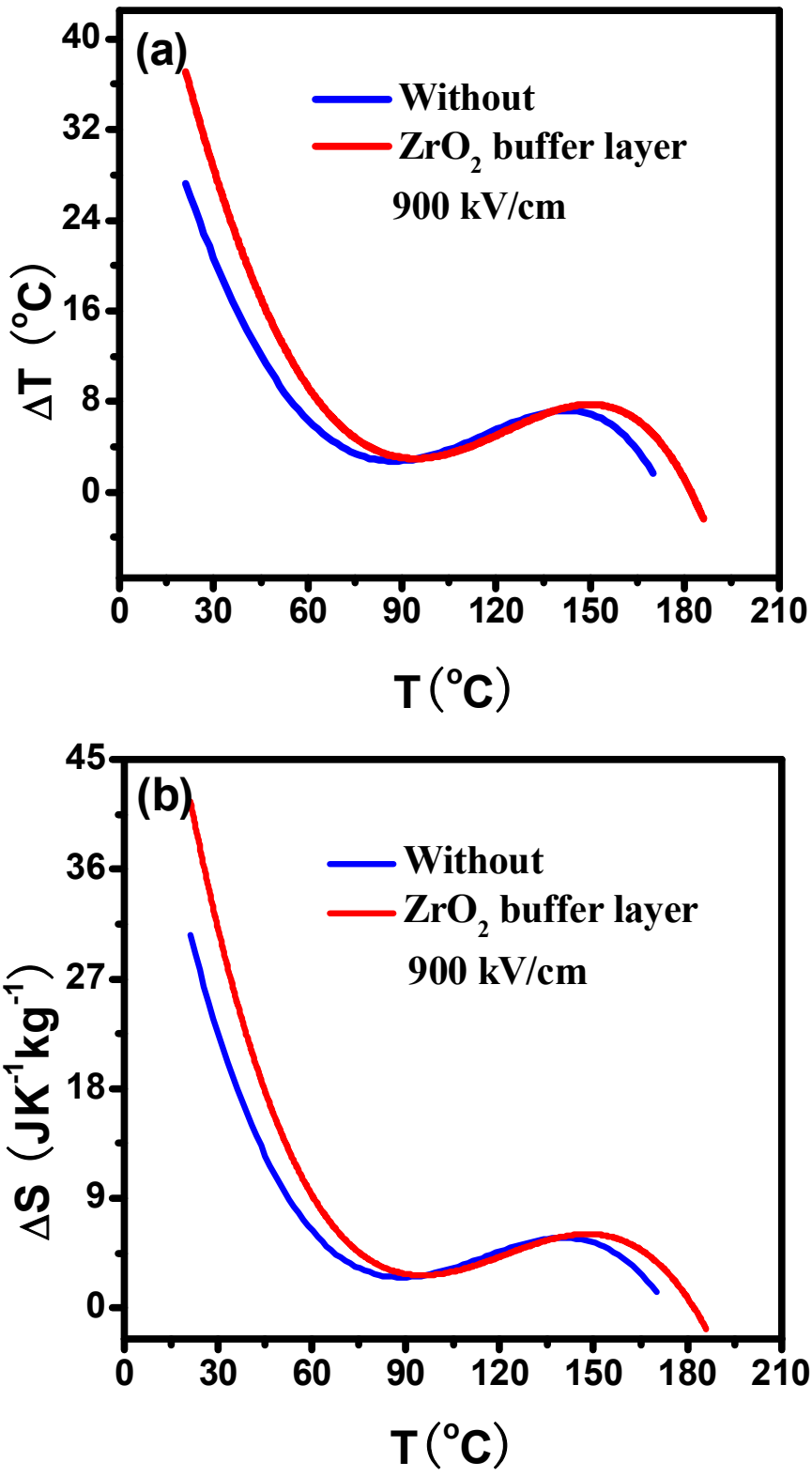

Fig. 5 Xihong Hao, and Ye Zhao, *et. al.*

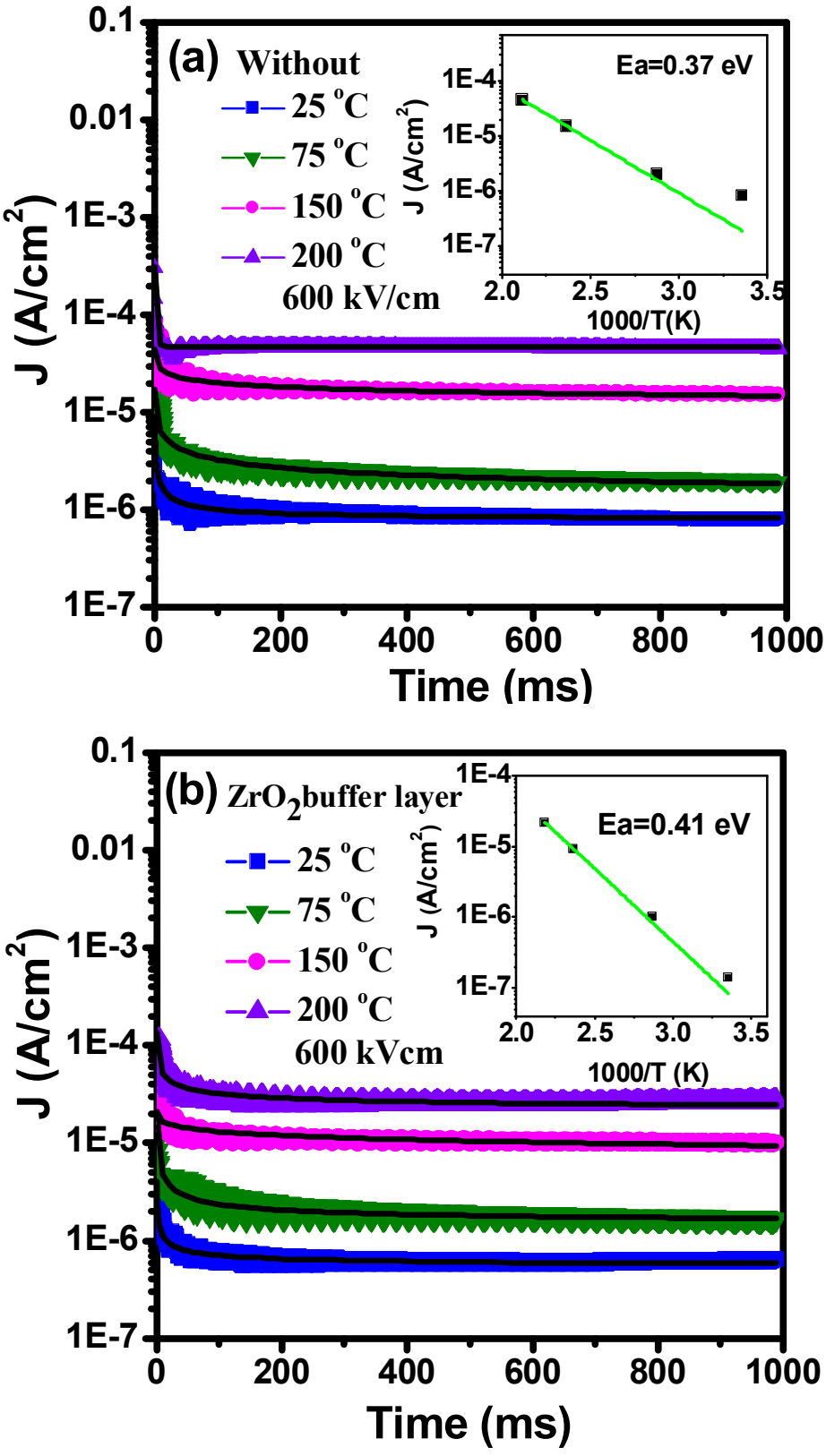

2015-09-09

# Improved electrocaloric effect in (100)-oriented Pb0.97La0.02(Zr0.57Sn0.38Ti0.05)O3 antiferroelectric thick film by interface engineering

Zhao, Ye

Elsevier